Crystal structure of pentameric shell protein CsoS4B of *Halothiobacillus neapolitanus* α-carboxysome

Yan-Yan Zhao, Yong-Liang Jiang, Yuxing Chen, Cong-Zhao Zhou[**], Qiong Li[*]

Hefei National Laboratory for Physical Sciences at the Microscale and School of Life Sciences, University of Science and Technology of China, Hefei, Anhui, 230026, China

ARTICLE INFO

ABSTRACT

Carboxysome, encapsulating an enzymatic core within an icosahedral-shaped semipermeable protein shell, could enhance CO_2 fixation under low CO_2 conditions in the environment. The shell of *Halothiobacillus neapolitanus* α-carboxysome possesses two 38% sequence-identical pentameric proteins, namely CsoS4A and CsoS4B. However, the functions of two paralogous pentameric proteins in α-carboxysome assembly remain unknown. Here we report the crystal structure of CsoS4B at 2.15 Å resolution. It displays as a stable pentamer, each subunit of which consists of a β-barrel core domain, in addition to an insertion of helix α1 that forms the central pore. Structural comparisons and multiple-sequence alignment strongly indicate that CsoS4A and CsoS4B differ from each other in interacting with various components of α-carboxysome, despite they share a similar overall structure. These findings provide the structural basis for further investigations on the self-assembly process of carboxysome.

© 2019 Elsevier Inc. All rights reserved.

1. Introduction

Bacterial microcompartments (BMCs) are functional analogs of eukaryotic organelles, sharing a common architecture of an enzymatic core encapsulated by a polyhedral and selectively permeable protein shell [1]. They spatially segregate the enzymes from the cytosol, providing an organized subcellular environment to concentrate metabolites, prevent unwanted side reactions and sequester toxic intermediates. BMCs found in 23 bacterial phyla could be classified into anabolic and catabolic BMCs, which are distributed in autotrophs and heterotrophs, respectively [2]. Carboxysome, the best-studied BMC, is the only known example of anabolic BMC. It was first isolated from *Halothiobacillus neapolitanus*, and functions to enhance CO_2 fixation in all cyanobacteria and some chemoautotrophic bacteria [3,4]. The carboxysome encapsulates two enzymes, carbonic anhydrase (CA) which converts bicarbonate to CO_2, and ribulose-1,5-carboxylase/oxygenase (RuBisCO) which catalyzes the key step in Calvin-Bensen-Bassham cycle by combining CO_2 and ribulose-1,5-bisphosphate to form two molecules of 3-phosphoglycerate [5]. The protein shell provides a selective barrier for the efflux of CO_2 and influx of O_2, elevates the local concentration of CO_2 around RuBisCO and minimizes the side reaction of RuBisCO with O_2 [6,7]. Therefore, carboxysomes enable efficient CO_2 fixation under low CO_2 conditions in the environment through the carbon-concentrating mechanism [8,9].

According to the type of RuBisCO and the pattern of gene organization, carboxysomes could be defined as α- and β-carboxysomes [4]. The α-carboxysome, found in marine cyanobacteria and some chemoautotrophs, encapsulates Form IA RuBisCO, whereas the β-carboxysome which is distributed in freshwater cyanobacteria encapsulates Form IB RuBisCO [10,11]. Genes encoding the components of α-carboxysome are always organized into a single operon, which is named *cso* operon and highly conserved in different species [4,12]. However, the genes for β-carboxysome are generally more dispersed throughout the genome and more variable among species, though some of the genes are clustered in *ccm* operon [13]. Both α- and β-carboxysomes have an icosahedral-shaped shell typically of 100—200 nm in diameter, and consist of three types of protein building blocks: BMC-H, BMC-T and BMC-P [1,14,15]. BMC-H protein, the most abundant type of shell protein, contains a Pfam00936 domain and assembles into the homohexamer; whereas the BMC-T protein, which is composed of two Pfam00936 domains in tandem, forms the trimer or so-called the pseudohexamer [16]. Pores formed at the symmetry axes of homohexamers and pseudohexamers provide channels for

---

metabolites to traverse the shell [5]. In contrast, the BMC-P protein consists of a Pfam03319 domain and forms the pentamer [17]. Previous studies indicated that BMC-H and BMC-T proteins constitute the flat facets of the polyhedral shell, and BMC-P proteins surrounded by hexamers form the vertices [18]. Each protein component of the shell has a concave and convex side, the former of which faces the cytosol [18].

In β-carboxysome, the pentameric BMC-P protein is termed CcmL, the deletion of which leads to an elongated and rod-shaped carboxysome [19]. To date, crystal structures of CcmL from several species have been solved, and structural analyses showed that the five subunits of CcmL pack against each other tightly to form a pentamer, leaving a narrow pore of ~5 Å in diameter at the center [17]. However, compared with the well-studied CcmL in β-carboxysome, studies on its counterpart in α-carboxysome are limited. The α-carboxysome typically possesses two paralogous pentameric proteins, namely CsoS4A and CsoS4B, which share a primary sequence identity of 38% in *H. neapolitanus*. Interestingly, in the absence of the *csoS4A* and *csoS4B* genes, despite the majority of α-carboxysomes in *H. neapolitanus* remain the icosahedral shape, the knockout strain is unable to grow under low CO_2 conditions [20]. The tertiary structure of CsoS4A from *H. neapolitanus* has been solved in 2008 [17], and it is the only pentameric shell protein of known structure in α-carboxysome. Structural comparison indicated that CsoS4A shares an overall structure similar to CcmL, but lacks two β strands at the C-terminus and owns a smaller central pore with a diameter of ~3.5 Å. Notably, regardless of size, the icosahedral shell of carboxysome just needs 12 pentamers to seal the vertices. The 3-D structure of CsoS4B from *H. neapolitanus*, and the reasons for pentameric protein redundancy in α-carboxysome remain unknown.

Here we solved the 2.15 Å crystal structure of CsoS4B, the other pentameric BMC-P protein in α-carboxysome in addition to the previously reported structure of CsoS4A. Each subunit of CsoS4B is composed of a β-barrel core domain and an inserted α helix, and the Loop$_{α1-β5}$ is quite flexible. Though CsoS4B most resembles its paralogous protein CsoS4A, structural comparisons suggested significant differences between CsoS4B and CsoS4A. The central pore of ~2.9 Å in diameter is not large enough for metabolites to traverse the shell. Furthermore, analyses of electrostatic potential strongly indicated that CsoS4B might interact with proteins encapsulated in α-carboxysome different from CsoS4A. These findings enabled us to propose that CsoS4A and CsoS4B probably function differently in the assembly of α-carboxysome.

2. Materials and methods

2.1. Cloning, expression, and purification

The coding region of CsoS4B (*hneap_0917*) was amplified from the plasmid pHnCBS1D deposited by David Savage at Addgene [21], and cloned into a modified pET29a vector with a C-terminal 6 × His-tag. The full-length protein was overexpressed in *Escherichia coli* Rosetta (DE3) strain (Novagen). Cells were grown at 37 °C in LB culture medium (10 g of NaCl, 10 g of tryptone, and 5 g of yeast extract per liter) containing 30 μg/mL kanamycin, and induced by 0.2 mM isopropy β-D-1-thiogalactopyranoside when the A_{600nm} reached 0.8. After growth for another 20 h at 16 °C, the cells were harvested and resuspended in 30 mL lysis buffer (20 mM Tris-HCl, pH 8.0, 100 mM NaCl, 5% glycerol and 5 mM β-mercaptoethanol), and then disrupted by 10 min of sonication. The supernatant containing the target protein was collected by centrifugation at 12,000×g for 30 min, and loaded onto a nickel-nitrilotriacetic acid column (GE Healthcare) equilibrated with the binding buffer, the same as the lysis buffer. The target protein was eluted with 500 mM

imidazole, and further purified by gel filtration (Superdex 75 column, GE Healthcare) in the binding buffer. The fractions containing the target protein were pooled and concentrated to 10 mg/mL by ultrafiltration. The purity of protein was assessed by gel electrophoresis.

To obtain CsoS4B crystals of good diffraction quality, we tried several truncations of CsoS4B. The plasmids were generated by a standard PCR-based strategy with the plasmid encoding the full-length CsoS4B as template. They were overexpressed and purified in the same manner as the full-length protein.

2.2. Crystallization, data collection, and processing

Both the full-length and truncated CsoS4B were applied to crystalliztion. Crystals were grown at 289 K using the sitting-drop vapor diffusion method by mixing 1 μL of protein solution with an equal volume of reservoir solution. The initial crystallization solution of the full-length CsoS4B is 0.5 M $NH_4H_2PO_4$, and 0.2 M sodium citrate, whereas that of CsoS4B$_{1-77}$ is 30% polyethylene glycol 400, 0.2 M Li_2SO_4 and 0.1 M sodium cacodylate pH 6.5. Then crystals were transferred to cryoprotectant (reservoir solution supplemented with 30% glycerol) and flash-cooled with liquid nitrogen. The X-ray diffraction data were collected at 100 K in a liquid nitrogen stream on beamline 17U at the Shanghai Synchrotron Radiation Facility using a EIGER X 16 M detector. All diffraction data were integrated and scaled with the program *HKL*2000 [22].

2.3. Structure determination and refinement

The crystal structure of CsoS4B$_{1-77}$ was determined by molecular replacement with *Molrep* program [23] in the *CCP4i* program suite [24] using the crystal structure of *H. neapolitanus* CsoS4A (PDB

Table 1
Crystal parameters, data collection, and structure refinement.

	CsoS4B
Data collection	
Wavelength (Å)	0.97918
Space group	*C*2
Unit cell parameters	
a, b, c (Å)	97.34, 68.43, 70.91
α, β, γ (°)	90.00, 124.42, 90.00
Resolution range (Å)[a]	50.00−2.15 (2.23−2.15)
Unique reflections	20, 226 (2, 011)
Completeness (%)	98.1 (98.5)
$<I/\sigma(I)>$	10.259 (3.41)
R_{merge}[b] (%)	18.7 (67.8)
Average redundancy	3.8 (3.3)
Structure refinement	
Resolution range (Å)	40.18−2.15
R_{factor}[c]/R_{free}[d] (%)	16.97/22.66
Number of protein atoms	2, 899
Number of water atoms	190
RMSD[e] bond lengths (Å)	0.009
RMSD bond angles (°)	1.52
Mean B factors (Å^2)	34.0
Ramachandran plot (residues, %)[f]	
Most favored (%)	98.12
Additional allowed (%)	1.88
Protein Data Bank entry	6JY5

[a] The values in parentheses refer to statistics in the highest bin.

[b] $R_{merge} = \sum_{hkl}\sum_i |I_i(hkl)-<I(hkl)>|/\sum_{hkl}\sum_i I_i(hkl)$, where $I_i(hkl)$ is the intensity of an observation, and $<I(hkl)>$ is the mean value for its unique reflection. Summations are over all reflections.

[c] $R_{factor} = \sum_h |Fo(h)-Fc(h)|/\sum_h Fo(h)$, where Fo and Fc are the observed and calculated structure-factor amplitudes, respectively.

[d] R_{free} was calculated with 5% of the data excluded from the refinement.

[e] RMSD from ideal values.

[f] Categories were defined by MolProbity.

entry 2rcf) as the search model [17]. The initial model was further refined by the maximum likelihood method implemented in *REFMAC*5 [25] as part of the *CCP*4i program suite [24], and rebuilt interactively with the program *Coot* [26]. The final model was evaluated with *MolProbity* [27] and wwPDB Validation Server [28]. The interface areas were calculated by PDBePISA [29]. All structure figures were prepared with *PyMOL* (https://pymol.org/2/).

2.4. Size exclusion chromatography with multi-angle light scattering (SEC-MALS)

The assays were performed through a Superdex 200 Increase 10/300 column (GE Healthcare) connected to the DAWN HELEOS II light scattering detector (Wyatt Technology) and the Optilab T-rEX refractive index detector (Wyatt Technology). The protein sample (100 μL, 1.0 mg/mL) was injected into and then eluted from the column, which was pre-equilibrated with the elution buffer (20 mM Hepes, pH 7.5, 100 mM NaCl). The results were recorded and processed by ASTRA 7.0.1 software (Wyatt Technology). The final graph was plotted using the Origin 8.1 software.

3. Results

3.1. Overall structure

We initially obtained crystals of the full-length CsoS4B, but after exhaustive optimization, the diffraction resolution is too low to determine the structure. Partial proteolysis combined with multiple-sequence alignment suggested a rather stable structure of a truncated version of CsoS4B (Met1-Asp77) excluding the most C-terminal four residues. We thus overexpressed and purified the

truncated protein, which was then subjected to crystallization screening. Eventually, we got high quality crystals of the truncated CsoS4B and solved the structure at 2.15 Å resolution in the space group *C2*. The CsoS4B structure is refined to final R and R_{free} values of 16.97% and 22.66%, respectively. The crystallographic parameters are listed in Table 1.

In the structure, each asymmetric unit contains five molecules of CsoS4B, forming a stable pentamer, which shapes roughly like a pentagonal disk with an edge length of ~32 Å (Fig. 1A). The pentamerization of CsoS4B in the crystal structure is in accordance with the results of SEC-MALS assays. As shown in Fig. 1B, the apparent molecular weight of CsoS4B is about 50 kDa, whereas the theoretical molecular weight of the monomer is 9.8 kDa, suggesting that CsoS4B exists as a pentamer in solution. Further analyses using PDBePISA [29] indicated that the two neighboring subunits of pentameric CsoS4B have a buried interface area of ~900 Å² in average, which is mainly stabilized by hydrogen bonds and salt bridges. In addition, like hexameric BMC-H and BMC-T proteins [1], the pentameric BMC-P protein CsoS4B also contains a concave side distinguished from the convex side.

Each subunit of CsoS4B consists of a β-barrel formed by five β strands, in addition to an inserted helix α1 between the strands β4 and β5 (Fig. 1A), in a topological architecture of β1-β2-β3-β4-α1-β5. Notably, an additional β strand formed by the C-terminal His-tag is visible in subunits B and D. The five subunits in the asymmetric unit share an overall structure similar to each other (Fig. 1C), with a root mean square deviation (RMSD) of 0.193–0.488 Å. The major difference comes from the loop connecting helix α1 and strand β5 (termed Loop$_{α1-β5}$), which protrudes to the convex side of CsoS4B (Fig. 1C). Previous structure of the intact shell from *Haliangium ochraceum* revealed that the convex side faces the lumen of BMC
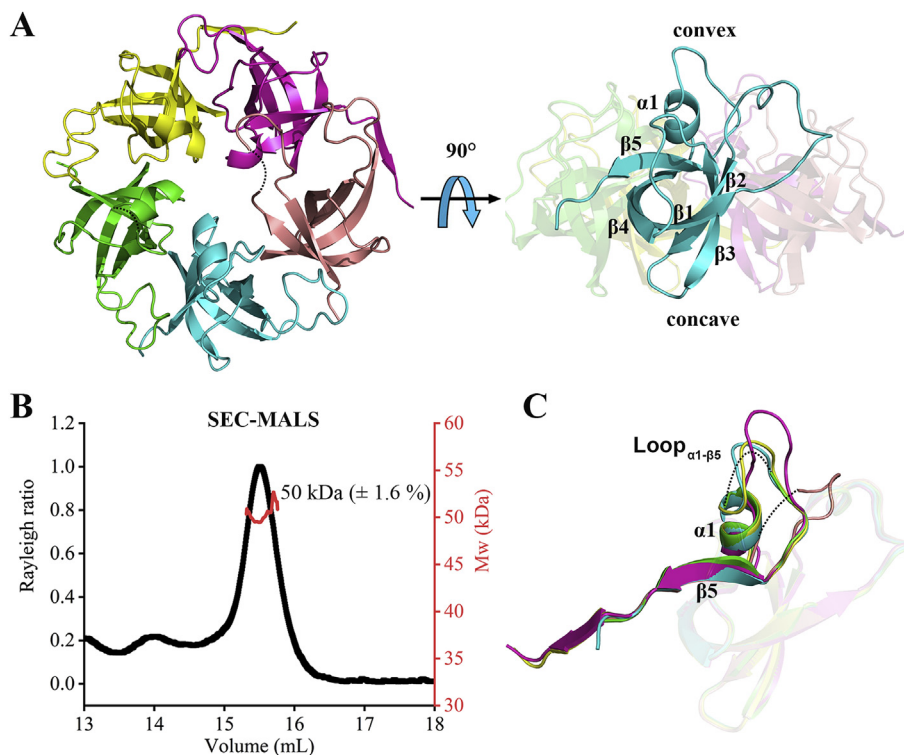

Fig. 1. Overall structure of CsoS4B. (A) Cartoon representation of pentameric CsoS4B in the top view (left) and side view (right). Five subunits (A to E) are colored in green, magenta, cyan, yellow and salmon, respectively. The disordered regions are shown as dotted lines. In the side view, subunit C is highlighted and labeled. (B) Analyses of SEC-MALS assays showed that CsoS4B exists as a pentamer in solution. The eluted peak is in correspondence with the X axis and the rayleigh ratio of the Y axis on the left. The jagged short line represents the molecular weight of the Y axis on the right. (C) Superposition of the five subunits against with each other. (For interpretation of the references to color in this figure legend, the reader is referred to the Web version of this article.)

[18]. Moreover, four residues (Val61-Phe64, corresponding to Loop$_{\alpha1-\beta5}$) of subunit A and six residues (Ala56-Val61, corresponding to helix α1 and part of Loop$_{\alpha1-\beta5}$) of subunit E couldn't be defined in the final model owing to the missing of electronic density, suggesting that Loop$_{\alpha1-\beta5}$ is flexible. Altogether, the structural flexibility and orientation of Loop$_{\alpha1-\beta5}$ indicated that CsoS4B might be involved in interaction with the encapsulated proteins or metabolites of α-carboxysome.

3.2. Structural comparisons

As mentioned above, the crystal structure of CsoS4A from *H. neapolitanus* was used as the search model for phase determination of CsoS4B. The DALI search [30] revealed that monomeric CsoS4B indeed has the highest structural homology to CsoS4A (PDB entry 2rcf, Z-score 14.0, sequence identity 38%), with an RMSD value of 1.6 Å over 77 Cα atoms. Superposition of the two structures

showed that they share a similar pentameric conformation (Fig. 2A). However, a close look at the monomeric structure revealed two major different regions: one is Loop$_{\alpha1-\beta5}$, the other one is the loop between strands β2 and β3 (termed Loop$_{\beta2-\beta3}$) (Fig. 2B). Notably, the two loops face opposite sides, the lumen of carboxysome and the cytosol, respectively. Besides, the strand β3 of CsoS4B is longer than that of CsoS4A (Fig. 2B). The structural differences indicated that though both as pentamers, CsoS4B might recognize and bind proteins or metabolites different from those of CsoS4A.

The crystal structure of an intact BMC shell from *H. ochraceum* presented the detailed interactions between hexamers and pentamers, which are primarily governed by complementarity in shape, in addition to few salt bridges and hydrogen bonds [18]. Structural analyses indicated that the intersubunit interactions are mainly contributed by seven residues in Loop$_{\beta1-\beta2}$, the GAGxGE and I(I/V)D motifs [18]. However, multiple-sequence alignment showed
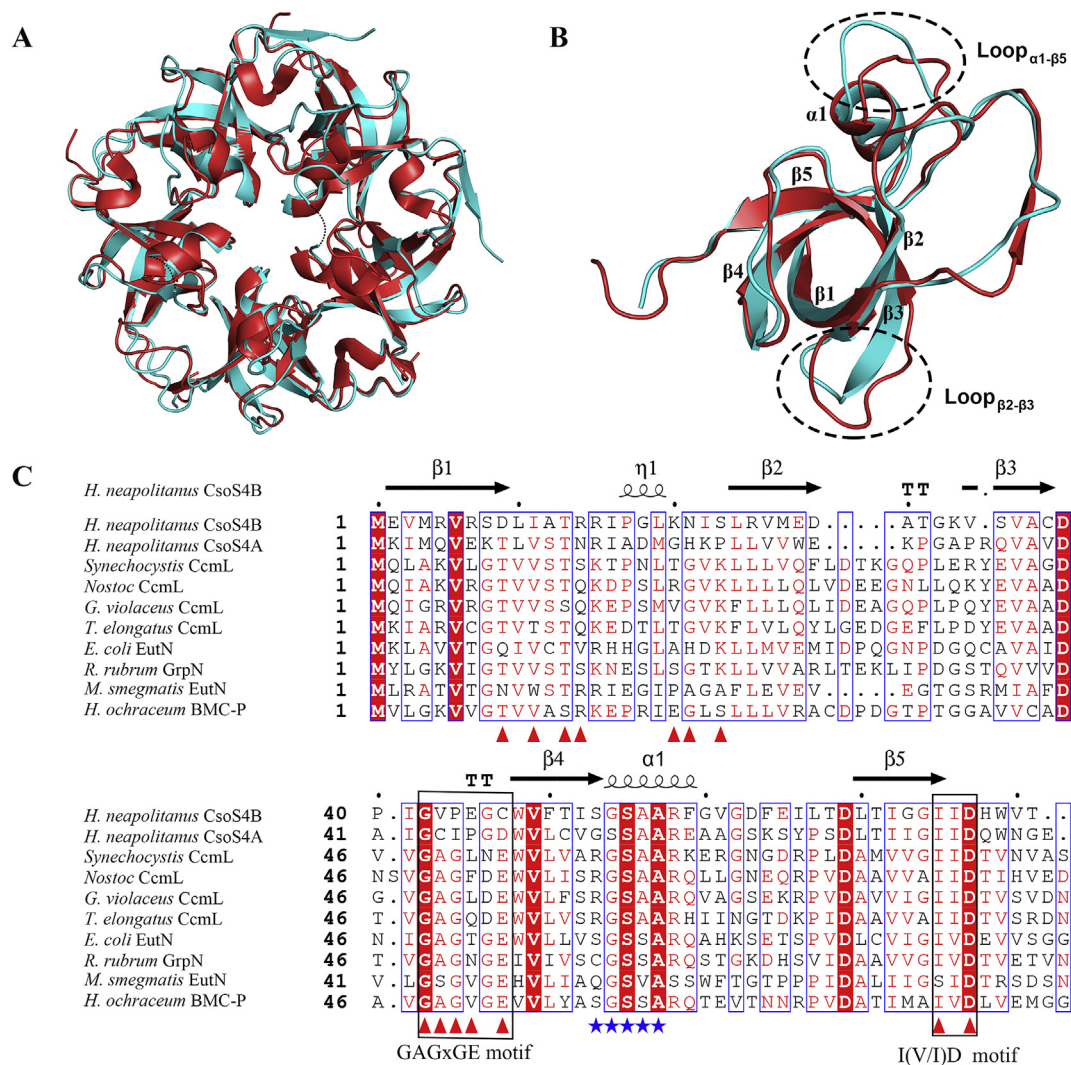

Fig. 2. Structural comparisons of CsoS4B against other BMC-P proteins. (A) Superposition of pentameric CsoS4B against CsoS4A. CsoS4A and CsoS4B are colored in red and cyan, respectively. (B) Superposition of CsoS4B monomer against CsoS4A monomer. The different loops are highlighted in dotted circle. (C) Multiple-sequence alignment of CsoS4B and BMC-P proteins with known structures. The alignment was performed with the programs Multalin and Espript. The secondary structural elements of CsoS4B are shown above the sequences. Residues involved in interacting with the BMC-H protein and forming the pore are marked with red triangles and blue asterisks, respectively. All sequences were downloaded from the Uniprot database (https://www.uniprot.org/) with the following accession numbers: *H. neapolitanus* CsoS4B, D0KZ87; *H. neapolitanus* CsoS4A, D0KZ88; *Synechocystis* PCC6803 CcmL, P72759; *Nostoc* PCC7120 CcmL, Q8YYI2; *Gloeobacter violaceus* CcmL, Q7NIT8; *Thermosynechococcus elongatus* CcmL, Q8DKB4; *E. coli* EutN, P0AEJ8; *Rhodospirillum rubrum* GrpN, Q2RVY2; *Mycobacterium smegmatis* EutN, A0QP50; *H. ochraceum* BMC-P, D0LHE5. (For interpretation of the references to color in this figure legend, the reader is referred to the Web version of this article.)

that except for the I(I/V)D motif, other interacting residues in CsoS4B corresponding to Loop$_{β1-β2}$ and the GAGxGE motif have somewhat low conservation, even compared with CsoS4A (Fig. 2C), suggesting that CsoS4B might interact with the hexameric shell proteins in a way different from that of CsoS4A or pentameric proteins of other BMCs.

3.3. The central pore

Along the central symmetry axis of pentameric CsoS4B, there is a pore surrounded by the hydroxyl group of Ser55 (Fig. 3A). Further structural analysis showed that Ser55, located at the N-terminal end of helix α1, is stabilized by Arg58 of the adjacent subunit through hydrogen bond (Fig. 3A). Notably, due to missing of helix α1 in subunit E, the central pore is somewhat deformed. In addition, the pore-forming residues S-G-S-A-A display some conservation with other pentameric proteins (Fig. 2C), but are less conserved compared to those in the hexameric shell proteins [31]. The diameter of the pore at the narrowest constriction site is ~2.9 Å (Fig. 3B), which is a bit smaller than that of CsoS4A (~3.5 Å) [17]. The central pore is thought to be a key feature of BMC shell proteins, and previous reports have proposed that the pores of hexamers and pseudohexamers function as conduits for metabolites to traverse the BMCs [5]. However, the minimum pore diameter of CsoS4B is much smaller than those of hexameric and pseudohexameric proteins, which are 4—7 Å and 13—14 Å in diameter, respectively [32]. Therefore, the pores of CsoS4B probably do not serve as conduits to allow metabolites to flow into and out of α-carboxysomes.

3.4. The electrostatic potential

Despite high structural similarities between CsoS4A and CsoS4B, the electrostatic potentials are distinctly different. In general, the electrostatic potential of CsoS4B is less basic than that of CsoS4A (Fig. 4). For example, two negatively charged residues Glu28 and Asp29 and one positively charged residue Lys33 contribute to an acidic concave side of CsoS4B, whereas one negatively charged residue Glu29 and three positively charged residues Lys8, Lys30 and Arg35 lead to a basic concave side of CsoS4A. In addition, Asp63 and Glu65 in the Loop$_{α1-β5}$ make the convex side of CsoS4B be acidic, but Lys65 in the corresponding region of CsoS4A results in a basic convex side. Moreover, the central pore of CsoS4A is more basic than that of CsoS4B (Fig. 4), which is due to a mutation of Lys2 to Glu2 (Fig. 2C). These differences indicated that CsoS4B might interact with proteins or metabolites different from those of CsoS4A.
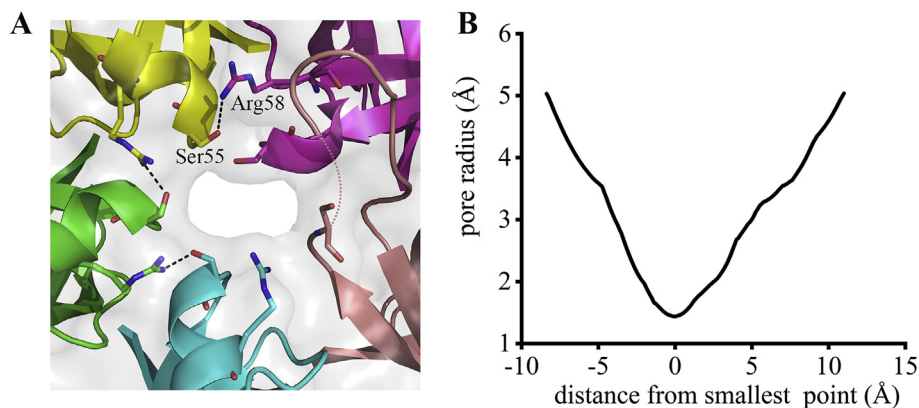

Fig. 4. Electrostatic potentials of CsoS4B and CsoS4A. The concave, convex and cross-section views are shown. The cross-section is sliced through the central pore. Red denotes negative charge; blue denotes positive charge.

4. Discussion

Though the facets of icosahedral-shaped BMC shell are composed of thousands of copies of hexameric BMC-H proteins, only 12 copies of pentameric BMC-P proteins are needed to seal the vertices of BMC shell [18]. However, α-carboxysomes in autotrophic bacteria and BMCs in heterotrophic bacteria usually contain multiple copies of genes encoding pentameric BMC-P proteins [2]. And in a previous research, bioinformatical analyses revealed that each genome contains 1.2 BMC-P genes on average per BMC Locus, among which the most extreme example is *Melioribacter roseus* P3M-2 with seven BMC-P genes [2]. The reasons for BMC-P protein redundancy in one species remain unknown.

Although the tertiary structure of CsoS4B we reported here is similar to that of CsoS4A, the redundant BMC-P protein in α-

Fig. 3. The central pore of CsoS4B. (A) A close view of the central pore from the convex side. Residues Ser55 and Arg58 are shown as sticks. Hydrogen bonds are indicated as black dotted lines. Due to the absence of helix α1 in subunit E, the hydrogen bonds between subunits E and C and subunits E and B are invisible. (B) Radius of the central pore plotted as a function of vertical position along the pore. The radius was calculated by the program HOLE2 [34].
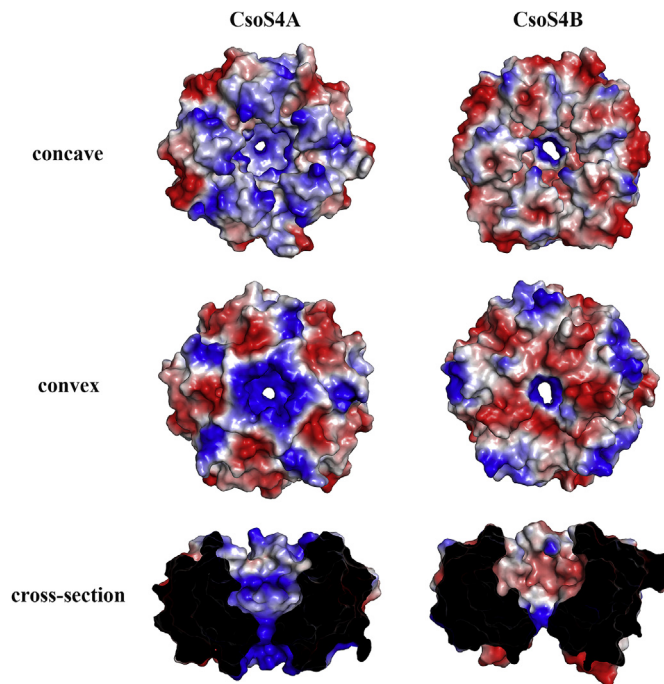
carboxysome, obvious differences could be seen, especially the electrostatic potential. These differences enabled us to propose a hypothesis that in addition to CsoS4A, CsoS4B helps to anchor different proteins or metabolites. As we know, proteins encapsulated in the lumen of α-carboxysome include enzymes RuBisCO and CA, and an intrinsically disordered protein CsoS2, which might function as a scaffold for the assembly of α-carboxysome [33]. The yeast two-hybrid assays showed strong interactions between CsoS4B and CsoS2 in both directions, whereas weak interactions between CsoS4A and CsoS2 only in one direction [33]. Moreover, CsoS2 has an isoelectric point (pI) value of 9.06, complementary to the acidic convex side of CsoS4B. But the pI values of RuBisCO and CA are about 6, reminiscent of the basic convex side of CsoS4A. These suggested that CsoS4B probably interact with encapsulating proteins different from CsoS4A. In addition, multiple-sequence alignment indicated that CsoS4A and CsoS4B might interact with hexameric shell proteins in a different way (Fig. 2C). Altogether, we proposed that the two redundant pentameric BMC-P proteins, CsoS4A and CsoS4B, might play distinct roles in α-carboxysome assembly. However, more structural and biochemical investigations are needed to clearly elucidate the roles of BMC-P proteins in the self-assembly process of BMCs.

Funding

Acknowledgements

References

[1] C.A. Kerfeld, C. Aussignargues, J. Zarzycki, F. Cai, M. Sutter, Bacterial microcompartments, Nat. Rev. Microbiol. 16 (2018) 277–290.
[2] S.D. Axen, O. Erbilgin, C.A. Kerfeld, A taxonomy of bacterial microcompartment loci constructed by a novel scoring method, PLoS Comput. Biol. 10 (2014), e1003898.
[3] J.M. Shively, F. Ball, D.H. Brown, R.E. Saunders, Functional organelles in prokaryotes: polyhedral inclusions (carboxysomes) of Thiobacillus neapolitanus, Science 182 (1973) 584–586.
[4] B.D. Rae, B.M. Long, M.R. Badger, G.D. Price, Functions, compositions, and evolution of the two types of carboxysomes: polyhedral microcompartments that facilitate CO₂ fixation in cyanobacteria and some proteobacteria, Microbiol. Mol. Biol. Rev. 77 (2013) 357–379.
[5] A. Turmo, C.R. Gonzalez-Esquer, C.A. Kerfeld, Carboxysomes: metabolic modules for CO₂ fixation, FEMS Microbiol 364 (2017) fnx176.
[6] S. Heinhorst, E.B. Williams, F. Cai, C.D. Murin, J.M. Shively, G.C. Cannon, Characterization of the carboxysomal carbonic anhydrase CsoSCA from Halothiobacillus neapolitanus, J. Bacteriol. 188 (2006) 8087–8094.
[7] M. Hagemann, A.R. Fernie, G.S. Espie, R. Kern, M. Eisenhut, S. Reumann, H. Bauwe, A.P. Weber, Evolution of the biochemistry of the photorespiratory C2 cycle, Plant Biol. (Stuttg) 15 (2013) 639–647.
[8] A. Kaplan, L. Reinhold, CO₂ concentrating mechanisms in photosynthetic microorganisms, Annu. Rev. Plant Physiol. Plant Mol. Biol. 50 (1999) 539–570.
[9] G.C. Cannon, C.E. Bradburne, H.C. Aldrich, S.H. Baker, S. Heinhorst, J.M. Shively, Microcompartments in prokaryotes: carboxysomes and related polyhedra, Appl. Environ. Microbiol. 67 (2001) 5351–5361.
[10] F.R. Tabita, Microbial ribulose 1,5-bisphosphate carboxylase/oxygenase: a different perspective, Photosynth. Res. 60 (1999) 1–28.
[11] M.R. Badger, E.J. Bek, Multiple Rubisco forms in proteobacteria: their functional significance in relation to CO₂ acquisition by the CBB cycle, J. Exp. Bot. 59 (2008) 1525–1541.
[12] G.C. Cannon, S.H. Baker, F. Soyer, D.R. Johnson, C.E. Bradburne, J.L. Mehlman, P.S. Davies, Q.L. Jiang, S. Heinhorst, J.M. Shively, Organization of carboxysome genes in the thiobacilli, Curr. Microbiol. 46 (2003) 115–119.
[13] G.D. Price, S.M. Howitt, K. Harrison, M.R. Badger, Analysis of a genomic DNA region from the cyanobacterium Synechococcus sp. strain PCC7942 involved in carboxysome assembly and function, J. Bacteriol. 175 (1993) 2871–2879.
[14] M.F. Schmid, A.M. Paredes, H.A. Khant, F. Soyer, H.C. Aldrich, W. Chiu, J.M. Shively, Structure of Halothiobacillus neapolitanus carboxysomes by cryo-electron tomography, J. Mol. Biol. 364 (2006) 526–535.
[15] C.V. Iancu, H.J. Ding, D.M. Morris, D.P. Dias, A.D. Gonzales, A. Martino, G.J. Jensen, The structure of isolated Synechococcus strain WH8102 carboxysomes as revealed by electron cryotomography, J. Mol. Biol. 372 (2007) 764–773.
[16] T.O. Yeates, C.A. Kerfeld, S. Heinhorst, G.C. Cannon, J.M. Shively, Protein-based organelles in bacteria: carboxysomes and related microcompartments, Nat. Rev. Microbiol. 6 (2008) 681–691.
[17] S. Tanaka, C.A. Kerfeld, M.R. Sawaya, F. Cai, S. Heinhorst, G.C. Cannon, T.O. Yeates, Atomic-level models of the bacterial carboxysome shell, Science 319 (2008) 1083–1086.
[18] M. Sutter, B. Greber, C. Aussignargues, C.A. Kerfeld, Assembly principles and structure of a 6.5-MDa bacterial microcompartment shell, Science 356 (2017) 1293–1297.
[19] G.D. Price, M.R. Badger, Isolation and characterization of high CO₂-requiring-mutants of the cyanobacterium Synechococcus PCC7942 : two phenotypes that accumulate inorganic carbon but are apparently unable to generate CO₂ within the carboxysome, Plant Physiol. 91 (1989) 514–525.
[20] F. Cai, B.B. Menon, G.C. Cannon, K.J. Curry, J.M. Shively, S. Heinhorst, The pentameric vertex proteins are necessary for the icosahedral carboxysome shell to function as a CO₂ leakage barrier, PLoS One 4 (2009), e7521.
[21] W. Bonacci, P.K. Teng, B. Afonso, H. Niederholtmeyer, P. Grob, P.A. Silver, D.F. Savage, Modularity of a carbon-fixing protein organelle, Proc. Natl. Acad. Sci. U.S.A. 109 (2012) 478–483.
[22] Z. Otwinowski, W. Minor, Processing of X-ray diffraction data collected in oscillation mode, Methods Enzymol. 276 (1997) 307–326.
[23] A. Vagin, A. Teplyakov, Molecular replacement with MOLREP, Acta Crystallogr. D Struct. Biol. 66 (2010) 22–25.
[24] N. Collaborative, Computational Project, the CCP4 suite: programs for protein crystallography, Acta Crystallogr. D Biol. Crystallogr. 50 (1994) 760–763.
[25] G.N. Murshudov, A.A. Vagin, E.J. Dodson, Refinement of macromolecular structures by the maximum-likelihood method, Acta Crystallogr, D Biol. Crystallogr. 53 (1997) 240–255.
[26] P. Emsley, K. Cowtan, Coot: model-building tools for molecular graphics, Acta Crystallogr. D Biol. Crystallogr. 60 (2004) 2126–2132.
[27] I.W. Davis, A. Leaver-Fay, V.B. Chen, J.N. Block, G.J. Kapral, X. Wang, L.W. Murray, W.B. Arendall 3rd, J. Snoeyink, J.S. Richardson, D.C. Richardson, MolProbity: all-atom contacts and structure validation for proteins and nucleic acids, Nucleic Acids Res. 35 (2007) W375–W383.
[28] H. Berman, K. Henrick, H. Nakamura, Announcing the worldwide protein data bank, Nat. Struct. Biol. 10 (2003) 980.
[29] E. Krissinel, K. Henrick, Inference of macromolecular assemblies from crystalline state, J. Mol. Biol. 372 (2007) 774–797.
[30] L. Holm, L.M. Laakso, Dali server update, Nucleic Acids Res. 44 (2016) W351–W355.
[31] J.N. Kinney, S.D. Axen, C.A. Kerfeld, Comparative analysis of carboxysome shell proteins, Photosynth. Res. 109 (2011) 21–32.
[32] M.J. Lee, D.J. Palmer, M.J. Warren, Biotechnological advances in bacterial microcompartment technology, Trends Biotechnol. 37 (2019) 325–336.
[33] F. Cai, Z. Dou, S.L. Bernstein, R. Leverenz, E.B. Williams, S. Heinhorst, G.C. Cannon, C.A. Kerfeld, Advances in understanding carboxysome assembly in Prochlorococcus and Synechococcus implicate CsoS2 as a critical component, Life (Basel) 5 (2015) 1141–1171.
[34] O.S. Smart, J.M. Goodfellow, B.A. Wallace, The pore dimensions of gramicidin A, Biophys. J. 65 (1993) 2455–2460.